THE JOURNAL OF BIOLOGICAL CHEMISTRY VOL. 286, NO. 36, pp. 31241–31249, September 9, 2011

Trafficking of α4* Nicotinic Receptors Revealed by Superecliptic Phluorin

EFFECTS OF A β4 AMYOTROPHIC LATERAL SCLEROSIS-ASSOCIATED MUTATION AND CHRONIC EXPOSURE TO NICOTINE[*][S]

Received for publication, April 29, 2011, and in revised form, July 13, 2011 Published, JBC Papers in Press, July 18, 2011, DOI 10.1074/jbc.M111.256024

Christopher I. Richards[1], **Rahul Srinivasan**[2], **Cheng Xiao, Elisha D. W. Mackey, Julie M. Miwa, and Henry A. Lester**[3]

From the Division of Biology, California Institute of Technology, Pasadena, California 91125

We employed a pH-sensitive GFP analog, superecliptic phluorin, to observe aspects of nicotinic acetylcholine receptor (nAChR) trafficking to the plasma membrane (PM) in cultured mouse cortical neurons. The experiments exploit differences in the pH among endoplasmic reticulum (ER), trafficking vesicles, and the extracellular solution. The data confirm that few α4β4 nAChRs, but many α4β2 nAChRs, remain in neutral intracellular compartments, mostly the ER. We observed fusion events between nAChR-containing vesicles and PM; these could be quantified in the dendritic processes. We also studied the β4R348C polymorphism, linked to amyotrophic lateral sclerosis (ALS). This mutation depressed fusion rates of α4β4 receptor-containing vesicles with the PM by ~2-fold, with only a small decrease in the number of nAChRs per vesicle. The mutation also decreased the number of ER exit sites, showing that the reduced receptor insertion results from a change at an early stage in trafficking. We confirm the previous report that the mutation leads to reduced agonist-induced currents; in the cortical neurons studied, the reduction amounts to 2–3-fold. Therefore, the reduced agonist-induced currents are caused by the reduced number of α4β4-containing vesicles reaching the membrane. Chronic nicotine exposure (0.2 μM) did not alter the PM insertion frequency or trafficking behavior of α4β4-laden vesicles. In contrast, chronic nicotine substantially increased the number of α4β2-containing vesicle fusions at the PM; this stage in α4β2 nAChR up-regulation is presumably downstream from increased ER exit. Superecliptic phluorin provides a tool to monitor trafficking dynamics of nAChRs in disease and addiction.

Nicotinic acetylcholine receptors (nAChRs)[4] are cation-selective transmembrane receptors expressed throughout the peripheral and central nervous systems (1, 2) and are assembled from various subunits (α1–α10, β2–β4, γ, δ, and ε). Because they function only when inserted into the plasma membrane (PM), nAChRs have been extensively studied with electrophysiology, yielding information about gating dynamics, ligand-induced activation, and desensitization (3–5). Although ideal for understanding function at the membrane, electrophysiology provides a limited understanding of intracellular receptor dynamics. Therefore, recent studies have used fluorescence-based imaging, primarily FRET-based and localization measurements, to complement previous biochemical data (6, 7) providing further insight into the assembly and trafficking of receptors (8–11).

Since 1998, superecliptic phluorin (SEP), a pH-sensitive analog of GFP, has been used to study vesicle dynamics and synaptic delivery (12, 13). It has also been used to study the trafficking of neurotransmitter receptors, such as AMPA and GABA receptors (14–17), to and from the PM. To date, this technique has not been applied to the study of nAChR dynamics. The application of SEP-based experiments for nAChRs allows direct monitoring of nAChR trafficking behavior influenced by drug exposure and/or mutations within the coding sequence. Such a tactic requires fusion of SEP to the extracellularly exposed N- or C-terminal region of an nAChR subunit; because SEP is in fact a modified GFP moiety, we were encouraged by previous reports that C- and N-terminal fusion constructs of nAChRs and other Cys-loop receptors exhibited function on the PM, albeit with some deficits (8, 10, 11, 18–23). Here, we incorporated a pH-sensitive fluorescent protein into the C terminus of the α4 subunit, then examined subcellular distribution of nicotinic receptors, and directly monitored receptor trafficking in real time.

We report SEP measurements to study nAChR trafficking in two disease-related contexts. First, ALS involves loss of cortical and motor neurons and eventually progresses to muscle paralysis and debilitation (24–27). Mutations of β4 subunits are associated with ALS (28, 29). One such mutation is adjacent to an L*X*M sequence, consisting of a putative ER exit motif in the

* This work was supported, in whole or in part, by National Institutes of Health Grants AG033954, DA17279, and NS11756. This work was also supported by the California Tobacco-related Disease Research Program Grant 19KT-0032 and by a gift from Louis and Janet Fletcher.

[S] The on-line version of this article (available at http://www.jbc.org) contains supplemental Figs. S1–S4.

[1] Supported by National Institutes of Health Kirschstein NRSA DA030877 and a Beckman Institute fellowship.

[2] Supported by a Tobacco-related Disease Research Program Postdoctoral Fellowship 18FT-0066 and by a Rapid Response grant from the Michael J. Fox Foundation.

[3] To whom correspondence should be addressed: Division of Biology, MC 156-29, California Institute of Technology, Pasadena, CA 91125. E-mail: lester@caltech.edu.

[4] The abbreviations used are: nAChR, nicotinic acetylcholine receptor; ALS, amyotrophic lateral sclerosis; SEP, superecliptic phluorin; eGFP, enhanced green fluorescent protein; ER, endoplasmic reticulum; TIRF, total internal reflection; ROI, region of interest; ERES, endoplasmic reticulum exit site; PM, plasma membrane; ACh, acetylcholine; pF, picofarad.

M3-M4 loop of β4. Mutant β4* receptors exhibit decreased agonist-induced whole cell currents compared with wild type receptors. Motifs in the M3-M4 loop of several nAChR subunits influence the targeting of receptors to subcellular compartments and therefore eventually promote or inhibit PM expression (21, 30, 31). For instance, when the β2 M3-M4 loop sequence is modified to incorporate an L*X*M ER motif mimicking that present in the β4 sequence, there is substantially decreased ER retention and increased PM localization of receptors (8). Smoking is linked to increased risk for sporadic ALS, and although the mechanistic basis is not understood, the recent identification of nAChR mutations linked to ALS suggests one of several possible links. We report that the ALS-associated β4R348C mutation changes the subcellular distribution of nAChRs and decreases the rate of insertion on the neuronal PM, and we confirm the previously reported decrement in agonist-induced currents.

Second, chronic exposure to nicotine is responsible for nicotine addiction (32, 33) and apparently also for a reduction in susceptibility to Parkinson's disease (34). Recent studies suggest that these effects proceed, at least partially, because nicotine acts as a pharmacological chaperone to enhance α4β2 nAChR formation (6, 7, 35–37). We report here that although chronic nicotine does not affect the rate of α4β4 insertion, it does produce enhanced insertion of α4β2 receptors.

EXPERIMENTAL PROCEDURES

Plasmid Constructs—Mouse α4 with a C-terminal fusion of an SEP tag was constructed by PCR amplification using the forward primer 5′-CATGGTTGGCTGGTATGATCAGTAAAGGAGAAGAACTT-3′ and the reverse primer 5′-ATGGATGAACTATACAAATAGGGAATAGCGGCACCT-3′, which overlap with sequences within the C-terminal end of the α4-coding sequence. This PCR product was then cloned directly into the vector containing the α4 gene using Pfu-Turbo polymerase. Mutations were introduced into the β4wt constructs with the forward primer 5′-AGCTGCCCACCTTCCTCTTCATGAAGTGCCCTGGTCTGGAAGTCAG-3′ and reverse primer 5′-CTGACTTCCAGACCAGGGCACTTCATGAAGAGGAAGGTGGGCAGCT-3′ and using the QuikChange II XL site-directed mutagenesis kit to create the β4R348C mutation. The Sec24D-enhanced YFP plasmid was provided by D. J. Stephens (University of Bristol School of Medical Sciences, Bristol, UK) (38). Sec24D-mCherry was cloned from Sec24DeYFP using the PCR integration method described above.

Cell Culture—Cortical neurons were extracted from day 17 mouse embryos and plated on 35-mm Mattek polylysine-coated glass bottom culture dishes in a neuronal medium containing Neurobasal, B27 (Invitrogen), and Glutamax supplemented with 3% equine serum. Neurons were plated at a density of 60,000 cells per dish. On day 4 of culture, neurons were treated with 1 μM cytosine arabinoside. Neurons were maintained via 50% exchange with feeding medium (Neurobasal, B27, and Glutamax) twice per week. On day 7 in culture, plasmids were mixed in 100 μl of OptiMEM, although 4 μl of Lipofectamine-2000 was mixed with a separate 100-μl aliquot of OptiMEM. After 5 min at 22 °C, the separate solutions were mixed together and kept at room temperature for an additional 25 min. Neurons were transfected with 750 ng of each nAChR plasmid and 350 of Sec24D-mCherry plasmid. After 3 h at 37 °C, transfection medium was replaced with neuronal feeding medium.

Mouse Neuro-2a cells were cultured using standard culture techniques and maintained in DMEM supplemented with 10% FBS. Cells were transfected with 500 ng of each nAChR plasmid. Cells were plated by adding 90,000 cells to poly-D-lysine-coated 35-mm glass-bottom imaging dishes (MatTek Corp.). The next day, plasmid DNA was mixed with cationic lipids by adding 500 ng of each nAChR plasmid to 4 μl of Expressfect transfection reagent in 200 μl of DMEM. After 20 min at room temperature, the transfection mixture was added to Neuro-2a cells in 1 ml of plating medium and incubated at 37 °C for 4 h. Dishes were rinsed twice with plating medium and incubated at 37 °C for 48 h.

TIRF Imaging—Cultured cortical neurons were imaged live 24 h after transfection at 37 °C in a stage-mounted culture dish incubator (Warner Instruments). TIRFM enables the visualization of fluorescently labeled intracellular molecules within 200 nm of the cell-coverslip interface. TIRF images were obtained using an inverted microscope (IX81; Olympus) equipped with an Olympus PlanApo 100× 1.45 NA oil objective and a stepper motor (Thorlabs) to control the position of the fiber optic and TIRF evanescent field illumination. The microscope includes a drift control module that maintains live cell samples at a constant focus for periods ≥24 h. Neuronal medium was exchanged for extracellular solution (ECS) (150 mM NaCl, 4 mM KCl, 10 mM HEPES, 2 mM $MgCl_2$, 2 mM $CaCl_2$, and 10 mM glucose) adjusted to the appropriate pH (5.4 or 7.4). SEP was excited with the 488-nm line of a multiline air-cooled argon laser (IMA101040ALS; Melles Griot). Images were captured with a back-illuminated EMCCD camera (iXON DU-897). Frame rates, laser power settings, and camera gain parameters were initially adjusted and then maintained constant across all samples for each imaging session. TIRF measurements to detect membrane insertion events were performed with consecutive 200-ms frames.

Insertion events were defined as punctate regions of fluorescence appearing at the membrane of dendritic processes. Regions exhibiting bright constant fluorescence features that can likely be attributed to ER (8) were excluded. Insertion event data are represented in terms of insertion per unit length of dendritic process measured per min of observation.

We acidified the imaging dish by perfusing the bath, normally at pH 7.4, with an otherwise identical solution adjusted to pH 5.4. The ratio of PM to ER expression was determined by taking an initial TIRF image of each neuron at pH 7.4 followed by acidification of the solution and a subsequent low-pH image. Two separate regions of interest were used to determine the subcellular distribution of fluorescent receptors in both the soma and the dendritic processes. A region of interest just encompassing the soma was internally thresholded to specifically demarcate only the cell body. A second ROI was drawn to exclude the cell body but include all visible processes. Internal thresholding was again used to select the processes above the background in this ROI. The ratio of the average intensities (fluorescence at pH 5.5/initial fluorescence at pH 7.4) indicates

the fraction of PM fluorescence; smaller values imply higher PM expression.

Confocal Imaging—An Eclipse C1si laser-scanning confocal microscope equipped with a 63× 1.4 NA VC Plan Apo oil objective and three individual photomultiplier tubes was used for confocal imaging. Before an imaging session, cell culture medium was replaced with phenol red-free CO_2-independent Leibovitz L-15 medium. All experiments were performed in live cells 24 h after transfection at 37 °C in a stage-mounted culture dish incubator (Warner Instruments). Cortical neurons exhibiting eGFP and mCherry fluorescence signals were acquired by excitation with 488 and 561 nm excitation, respectively. The fluorescence signal was detected by splitting the green and red emission with a dichroic filter and then directing the signal from each emissive species through the appropriate optical bandpass filters. We focused on a plane containing the most ERES in dendritic processes. Sequential images of eGFP and mCherry fluorescence were obtained at separate photomultiplier tubes. For quantification, ERES ROIs were demarcated using intensity-based thresholding and counted for each cell using the particle analysis feature in Metamorph 7 (8).

Whole Cell Patch Clamp Recordings—The Neuro-2a or cultured cortical cells were visualized with an upright microscope (BX50WI; Olympus) in either bright field or fluorescent (eGFP and mCherry) mode. Electrophysiological signals were recorded with a MultiClamp 700B amplifier (Axon Instruments, Molecular Devices, Union City, CA), Digidata 1322 analog-to-digital converters (Axon), and pCLAMP 9.2 software (Axon). The patch pipette resistances were 4–6 megohms, when filled with the following (mM): 135 potassium gluconate, 5 KCl, 5 EGTA, 0.5 $CaCl_2$, 10 HEPES, 2 Mg-ATP, and 0.1 GTP. The pH of these solutions was adjusted to 7.2 with Tris base, and the osmolarity to 300 mOsm with sucrose. The junction potential between the patch pipette and the bath solutions was nulled just before we formed the gigaseal. Series resistance was monitored without compensation throughout the experiment. The data were discarded if the series resistance (10–30 megohms) changed by >20% during recordings. Data were sampled at 10 kHz and filtered at 2 kHz. All recordings were done at 22 °C.

We puffed ACh (300 μM, 0.1 s) dissolved in extracellular solution (in mM: 140 NaCl, 5 KCl, 2 $CaCl_2$, 1 $MgCl_2$, 10 HEPES, and 10 glucose; 320 mosM, pH set to 7.3 with Tris base) onto the cells (holding potential, −65 mV). Current density was calculated as peak amplitude divided by membrane capacitance.

As in previous studies (10), we observe no ACh-induced currents in untransfected neurons at this stage in culture. As in previous studies (10), we assume that endogenous subunit populations are too small to distort our results by heteropolymerizing with the expressed fluorescent subunits.

RESULTS

We used SEP fused to the C terminus of α4 nicotinic receptor subunits to examine the subcellular distribution and trafficking dynamics of receptors expressed in cortical neurons. SEP is a pH-sensitive version of enhanced green fluorescent protein (eGFP) that undergoes 488 nm excitation at neutral pH (~7.4) but loses this excitation maximum under acidic conditions (12).

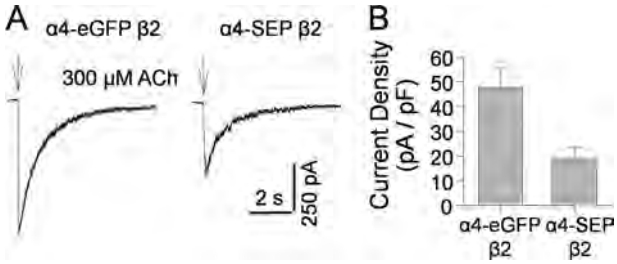

FIGURE 1. **α4-SEP forms functional nAChRs with β2 subunits in Neuro-2a cells.** *A,* typical traces of ACh responses in a cell transfected with α4-eGFPβ2 subunits and a cell transfected with α4-SEPβ2 subunits. These cells have similar PM capacitance (~20 pF). *B,* summary of ACh-induced current density of cells transfected with either α4-eGFPβ2 subunits (47.6 ± 7.8 pA/pF, $n = 4$) or α4-SEPβ2 subunits (18.9 ± 4.4 pA/pF, $n = 4$) ($p = 0.009$).

As a result, SEP neither photobleaches nor fluoresces at low pH but regains its fluorescence at neutral and basic pH. Tagging of α4 on the extracellular C terminus also results in the orientation of SEP on the lumenal side of most organelle types in the secretory pathway. Although the endoplasmic reticulum (ER) and *cis*-Golgi have lumenal pH values of ~7.2 and ~6.7, respectively, the lumen of the *trans*-Golgi network, secretory vesicles, and lysosomes is much more acidic (pH <6.5) (39). If one illuminates via TIRF microscopy, only those receptors resident in nearly neutral organelles close to the PM, or inserted in the PM, are visible within the excitation field. Thus, receptors in the later stages of the secretory pathway neither fluoresce nor photobleach due to the acidic environment. This arrangement allows us to visualize receptors as they are inserted into the PM, because the SEP moiety transitions from the acidic environment within the transport vesicle to the neutral pH of the extracellular solution.

To verify that α4-SEP subunits form functional receptors, we compared whole cell currents of α4-SEP β2wt and α4-eGFP β2wt in transiently transfected Neuro-2a cells (Fig. 1, *A* and *B*). The density of ACh-induced currents for α4-SEP β2 nAChR was 40% that seen for receptors with the M3-M4 insertion of eGFP (Fig. 1*B*). These data show that the receptors with a C-terminal FP fusion function, although less well than the control.

An epifluorescence image of a representative cortical neuron transfected with α4-SEP β4wt reveals fluorescence from all nonacidic compartments, *i.e.* from receptors at the membrane, in the ER, and in the *cis*-Golgi (Fig. 2*A*) (untransfected cells showed no detectable fluorescence). To determine the extent of PM expression, we adjusted the extracellular pH to 5.4. Because SEP is fused to the C terminus of α4, it senses the extracellular solution; therefore, a reduction in the pH results in the elimination of the membrane-based fluorescence signal. Emission from receptors residing in intracellular regions is initially unaffected by the change in extracellular pH. On addition of an acidic extracellular solution, the fluorescence intensity in the soma is clearly reduced (Fig. 2*B*) but is still quite prominent, indicating that a major population of receptors resides in the ER. This observation is entirely consistent with previous data for $\alpha4\beta2$ nAChRs in neurons and does not arise from artifacts due to tissue culture, trafficking, or microscopy (10, 40, 41). The distribution of receptors in the processes is rather different; many dendrites visible in the original image exhibited distinctly lower levels of fluorescence in the low-pH solution. Although

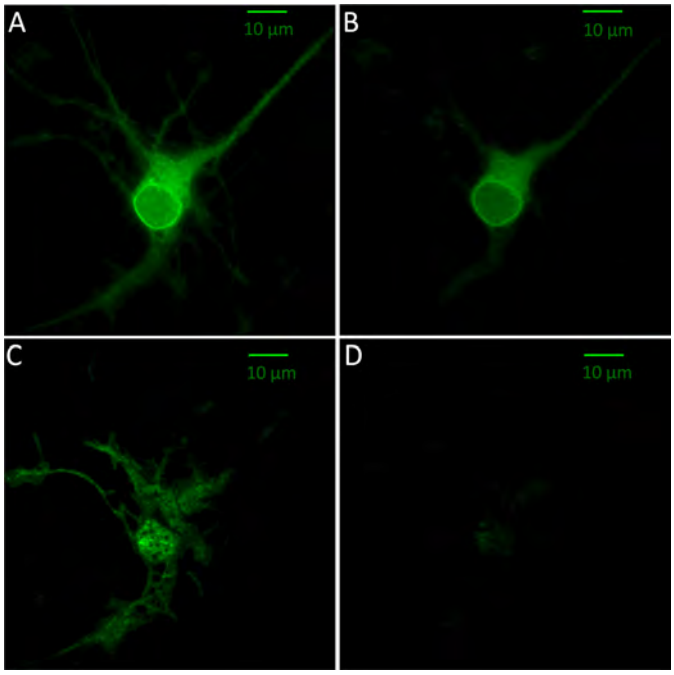

FIGURE 2. **SEP-labeled α4β4 nAChRs.** *A,* representative epifluorescence image of a cortical neuron (8 days in culture) expressing α4-SEP and β4wt with an extracellular pH of 7.4. *B,* same neuron depicted in *A*, after the extracellular solution was adjusted to pH 5.4. The images are acquired and shown at the same intensity scale. *C,* same neuron depicted in *A* and *B*, imaged with TIRF excitation at an extracellular pH of 7.4. *D,* TIRF image of the same neuron with an extracellular pH of 5.4. The intensity scale equals that of *C*.

receptors are still clearly visible in the processes, this marked fractional decrease in the fluorescence indicates that the processes have a proportionally smaller population of α4β4 nAChRs in neutral environments such as ER compared with the cell body. Because these images are taken with epifluorescence, even receptors residing 1 to 2 μm away from the PM would still be visible.

Fig. 2, *C* and *D,* shows TIRF images of the same neuron. The major observation is that the neuron exhibits robust fluorescence, with a typical membrane "footprint" pattern, at neutral pH but that this fluorescence is markedly diminished in the acidic solution. To verify that intracellular fluorescence originates from receptors retained in the ER, we cotransfected neurons with nAChRs and a dsRed-labeled ER-localized sequence (KDEL). Comparison of the nAChR signal (eGFP) and the ER signal reveals extensive colocalization (supplemental Fig. S1). This supports the usual interpretation that the intracellular fluorescence can be attributed to ER resident receptors. The data thus confirm and extend those of an earlier study, using fluorescent nAChRs with an alternative ER marker, which concluded that most intracellular nAChRs reside in the ER (8). It is possible that some ER fluorescence also arises from unassembled or partially assembled subunits, but SEP does not fluoresce in those subunits that are transported to lysosomes and other acidic catabolic vesicles.

We comment on the comparison between the epifluorescence (Fig. 2*A*) and TIRF (Fig. 2*C*) images. (1) The two images emphasize different aspects of cell structure. Where the TIRF image is relatively brighter than the epifluorescence image, we assume that most of the nAChRs reside near the coverslip. Some portions of dendrites are visible in epifluorescence but not in TIRF; presumably these regions extend away from the surface of the coverglass. (2) Typically, the TIRF excitation field extends ~200 nm in the axial direction. As a result, only the ER at the periphery of the cell is visible along with the PM fluorescence. With an acidic extracellular solution, TIRF excitation reveals that most of the fluorescence has been quenched, leaving a small but measurable fraction of residual fluorescence in the soma. This reduced fluorescence in TIRF images at acidic pH suggests that the majority of intracellular receptors are not in near-membrane neutral organelles but reside much deeper and that any dendritic ER contains low levels of α4β4 nAChRs.

If changes to extracellular pH do eventually affect intra-organelle pH, this distortion would presumably occur most strongly for organelles near the PM. This is a particular concern in the processes, as the small radius places most of the organelles <1 μm from the extracellular solution. To test the effects of the acidic extracellular solution on SEP fluorophores in the ER of the soma and dendrites, we performed a series of control experiments. As unassembled α4 subunits in the absence of a β subunit remain in the ER, we transfected neurons with only the α4-SEP. We then compared the fluorescence at neutral and acidic pH (supplemental Fig. S2). These controls showed no observable decrease in the fluorescent signal in either the soma or the dendrites. Therefore, the acidic extracellular solution on the time frame of our experiments (<5 min after solution change) does not affect the pH of the ER. (This result also shows that any endogenous β2 or β4 subunits are present in quantities too low to distort the data by associating with the heterologously expressed α4 subunits.) These points establish that it is feasible to employ SEP-nAChR fusions to measure surface insertion of nAChRs.

ER Exit and Plasma Membrane Insertion of α4β4 nAChRs Are Reduced by β4R348C Mutation—We introduced an Arg to Cys point mutation in the mouse β4 construct at position 348, a position adjacent to a putative LFM ER exit motif in the M3-M4 cytoplasmic loop (8). The aligning mutation in the human β4 is associated with ALS. The mutation yielded reduced ACh- and nicotine-induced currents when compared with the wild type construct (28), but it is not known whether this results from decreased trafficking of receptors to the PM. To study this point, we transiently transfected cortical neurons with α4-SEP β4wt and compared them to neurons transfected with an equal amount α4-SEP β4R348C. To gain further insight into differences in the subcellular distribution of α4β4, we took advantage of the pH sensitivity of the superecliptic phluorin tag on the C terminus of the α4 construct.

We were able to distinguish differences in the subcellular distribution of WT and mutant α4β4 receptors utilizing the pH sensitivity of the SEP moiety on the C terminus of the α4 construct. Although changes in total levels of fluorescence are more subtle than the electrophysiological studies that showed reduced agonist-induced currents for β4R348C receptors (28, 29), surveying individual cells at both neutral and acidic pH eliminates bias originating from large variations in expression levels among cells. Here, we also used ROIs to discriminate between the cell body and processes. Calculating the ratio of fluorescence at pH 5.4 to fluorescence at 7.4 provides a measure

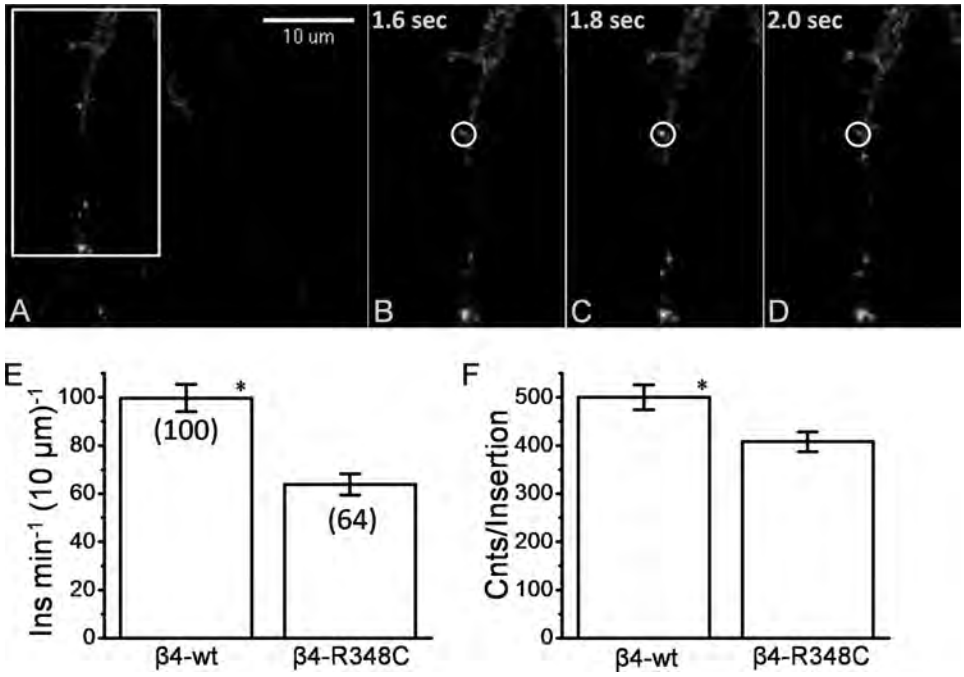

FIGURE 3. **Dynamic visualization of membrane insertion events.** *A,* TIRF image of dendritic processes of day 8 cortical neuron transfected with α4-SEPβ4wt and excited with a 488 nm laser with images taken at a frame rate of 200 ms. The *white box* is the region magnified in *B–D*. *B,* frame directly preceding an insertion event at the PM. *C,* frame showing the insertion of a vesicle containing α4-SEPβ4wt into the PM. *D,* frame directly after the observation of the insertion event. The *white circle* marks the location of the insertion in the previous frame. *E,* average insertions compared for α4-SEPβ4wt (six cells) and α4-SEPβ4-R348C (six cells). Insertion events are compiled for the neurites of each cell and calculated as number of insertions per 10 μm length of neurite per min. Number of insertions is indicated in *parentheses*. *F,* average intensity of insertion events, calculated as described under "Experimental Procedures." *Error bars* depict S.E. *NS,* not significant; *, $p < .05$.

of the extent of receptors in the ER as compared with those in the PM and is unaffected by receptors that are being actively trafficked to the PM as they are not fluorescent. We found that ~75% of the observable fluorescence in the soma of both wild type and mutant receptors was from plasma membrane resident receptors. Additionally, we found that the majority of the fluorescence in the dendrites was quenched at low pH, to the point that the processes became indistinguishable from the background. This suggests that there were no differences in the subcellular distribution of the mutant and wild type receptors, and in both cases most nAChRs reside at the PM and are not retained in the dendritic ER and/or *cis*-Golgi.

As superecliptic phluorin is not excited in an acidic environment, it does not undergo photobleaching during vesicular transport, but it exhibits a burst of fluorescence when exposed to the neutral extracellular solution as the vesicle merges with the PM during receptor insertion. This can be exploited to reveal trafficking dynamics. Additionally, the relative brightness of each insertion shows whether observed differences in PM levels result from an increase in the number of vesicles or an increase in the number of receptors per vesicle. To compare trafficking rates of α4β4wt and α4β4R348C, we used TIRF microscopy to monitor insertion rates in the processes of cortical neurons.

As seen from the pH dependence studies (Fig. 2), only a small fraction of the fluorescence observed in dendritic processes is due to ER resident nAChRs. In TIRF microscopy, insertion events are more readily visualized in the presence of lower levels of background fluorescence, and as a result insertion events in the processes are detected without interference from intracellular emission. We compared trafficking dynamics for the wild type and R348C mutant nAChRs.

Fig. 3*A* shows a dendrite of a cortical neuron transfected with α4-SEP β4wt and imaged with TIRF microscopy. A clear insertion event occurs at the PM, evidenced by the bright punctate feature. Three consecutive frames with 200-ms exposure reveal the time course of the insertion event. The initial frame (Fig. 3*B*) shows no bright features, although the next frame (200 ms later) (Fig. 3*C*) shows the arrival of a vesicle at the PM, which is apparent from the bright fluorescent feature outlined by the *white circle*. Just 200 ms after its arrival, the nAChRs have now recycled from the membrane as evidenced by the absence of the fluorescence feature. These events had an elevated fluorescence intensity characterized as a punctate region for 440 $\pm$ 83 ms (mean $\pm$ S.E., $n = 12$). The transient nature of the arrival event and the lack of observed spreading of the fluorescence from the concentrated punctate region indicate that the vesicle briefly encounters the PM and does not transfer all its nAChRs to the PM.

We quantified these data by counting the number of insertion events in the dendrites of the cortical neurons per linear distance of the dendrite per time increment. These data reveal marked differences between the WT receptors and the β4R348C* mutant receptors. Fig. 3*E* shows that the WT receptors are inserted at nearly twice the rate of the mutant receptors. From this, it is clear that the lower agonist-induced currents observed for cells transfected with the mutant receptors (28) arises at least partially from differences in trafficking to the PM.

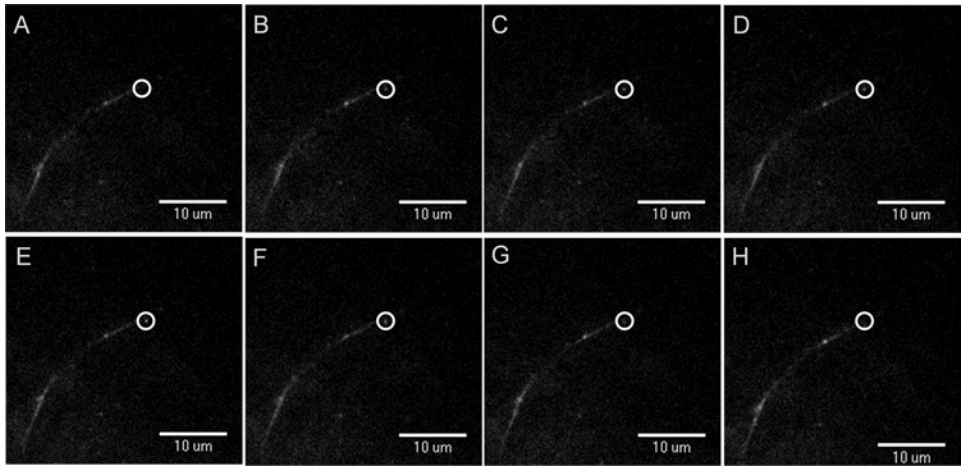

FIGURE 4. **Sustained PM insertion events.** *A–H,* consecutive frames (200-ms intervals) displaying TIRF images of a sustained insertion event in a dendritic process of a day 13 cortical neuron transfected with α4-SEPβ4wt and excited with a 488 nm laser. The *circle* shows the insertion event.

The intensity of the fluorescence burst associated with the insertion is proportional to nAChR numbers on the vesicles. We studied this parameter by taking the average fluorescence of the area demarcated by the ROI of the insertion from the frame preceding the arrival event and then subtracting this from the frame with the insertion event. Fig. 3*F* compares the intensity of the insertion events for the wild type *versus* the mutant receptors. The insertion events for the wild type receptors show slightly (25%) higher intensity than the mutant receptors. The wild type and mutant receptors had a similar fraction of sustained events compared with transient events. Although overall the wild type receptor exhibited approximately twice the number of insertions, the percentage of these that were observed to have persistent interaction (>1 s) was nearly identical for the wild type (4.3%) and mutant receptor (3.7%).

To examine if the longer persistent events (>1 s) resulted in the insertion of all receptors, we examined the time course of each event. Fig. 4 shows such a persistent insertion event. The consecutive frames taken every 200 ms show a clear insertion event that lasts >1 s, and the punctate increase becomes more diffuse, spreading within the PM (Fig. 4*H*). Although persistent events represented only a few percent of the total number of insertions, the majority of the longer interactions exhibited a diffusion of receptors away from the original puncta associated with the insertion event. This indicates that the more prolonged fusion events likely deposit most or all of their receptors on the membrane.

Because LFM motifs have been implicated in ER export of cargo, it is possible that a mutation in such close proximity to an L*X*M motif disrupts the normal trafficking through the secretory pathway. To further investigate this idea, we examined the effect of the β4R348C mutation on ERES, whose numbers have been shown to change with mutations in ER exit and retention motifs of α4β2 receptors (8). To observe differences in ERES, cortical neurons were cotransfected with α4-eGFP β4wt and the ERES marker, Sec24D labeled with mCherry. Confocal microscopy was used to observe areas where Sec24D has been recruited into ERES in the processes of neurons as seen in Fig. 5. ERES were defined as punctate regions that exhibited brighter fluorescence than the background mCherry fluorescence in the

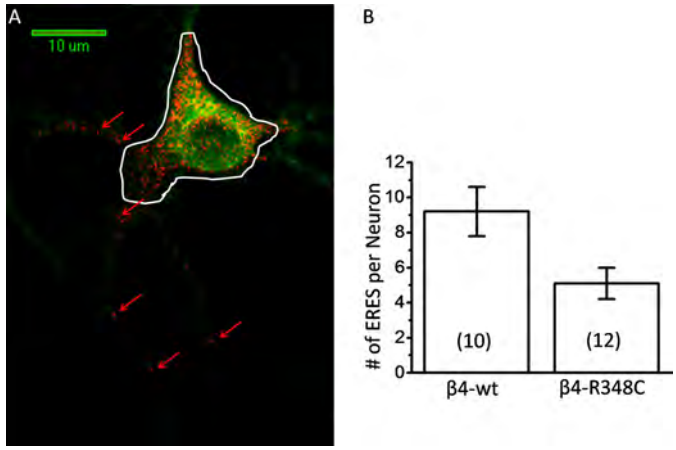

FIGURE 5. **Dendritic ERES comparison of α4-SEPβ4wt and α4-SEPβ4R348C.** Confocal imaging of day 8 mouse cortical neurons expressing Sec24D-mCherry with 561 nm excitation. ERES were counted as punctate regions of red channel fluorescence visible above any background fluorescence. *A,* representative confocal image of α4-eGFPβ4wt cotransfected with Sec24D-mCherry. *B,* average number of ERES in dendritic processes per neuron is represented for α4β4wt and α4-SEPβ4R348C. The number of cells is shown in *parentheses*. Channels were collected separately, and then a two-dimensional projection of a *z*-stack of the nAChR fluorescence was overlaid with the image of ERES. *Error bars* depict S.E. *NS,* not significant, and *, $p < 0.05$. The *white line* in *A* indicates the ROI used to distinguish the soma from the processes; ERES were counted outside the line boundary. The *red arrows* indicate representative ERES.

rest of the dendrite. Fig. 5 depicts a neuron transfected with α4-eGFP β4wt and Sec24D-mCherry. Several ERES can readily be observed throughout a major portion of the dendritic processes. The *white line* in Fig. 5*A* indicates the ROI used to distinguish the cell soma from the processes, and only ERES outside of the cell body were counted. Compared with mutant α4β4 nAChRs, we found significantly more ERES for cells expressing the wild type nAChRs. These differences further suggest that the ER exit of assembled α4β4 pentamers is interrupted by the R348C mutation.

ERES measurements in the soma are considerably less reliable than measurements in the processes. In 80% of the neurons, expression resulted in a very dense region of fluorescence, with many overlapping puncta, making it impossible to resolve individual ERES. Therefore, we report no ERES measurements for the somata.

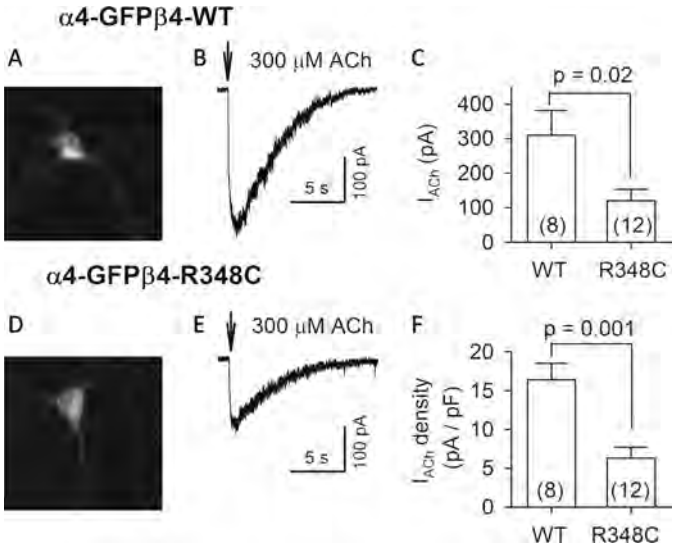

FIGURE 6. **ACh-evoked currents in neurons transfected with α4-eGFPβ4wt and α4-eGFPβ4-R348C nAChRs.** The transfected neurons were identified with green fluorescence (*A* and *D*). ACh (300 μM) was puffed (0.1 s) onto voltage-clamped neurons ($V_H = -65$ mV) and evoked inward currents (*B* and *E*). *C*, summary of 300 μM ACh-evoked currents (I_{ACh}) from neurons with different transfections (*WT*, α4-eGFPβ4wt; *R348C*, α4-eGFPβ4-R348C). *F*, summary of the density of 300 μM ACh-induced currents (I_{ACh} divided by membrane capacitance). Numbers of recorded neurons are indicated in *parentheses*.

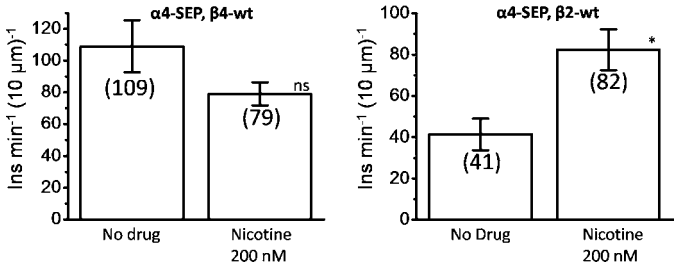

FIGURE 7. **Effect of nicotine on PM insertions for α4-SEPβ4wt and α4-SEPβ2wt.** *Left panel,* average measured insertion events for α4-SEPβ4wt calculated as insertion events/μm of linear neurite section/min, comparing cells without drug (6 cells) to those incubated with 200 nM nicotine (6 cells) for 24 h. *Right panel,* average measured insertion events for α4-SEPβ2wt calculated as insertion events/10 μm of neurite length/min. Cells without drug (five cells) are compared with those incubated with 200 nM nicotine (four cells) for 24 h. Number of insertions are indicated in *parentheses*. *Error bars* depict S.E. *NS*, not significant, and *, $p < 0.05$.

Agonist-evoked Currents Are Reduced by the β4R348C Mutation—That the wild type receptors are inserted at nearly twice the rate of the mutant channels (Fig. 3*E*) does not explain the ~10-fold difference in agonist-induced currents previously reported when the wild type and mutant nAChRs were compared by expression in a clonal cell line (22, 23). To correlate the fluorescence-based insertion measurements with electrophysiological measurements, we performed whole cell patch clamp recording from neurons in the preparation used for our fluorescence experiments. Neurons were transfected either with α4-eGFP β4wt or with α4-eGFP β4R348C nAChRs. The successfully transfected neurons were identified with green fluorescence (Fig. 6, *A* and *D*). Puffs of 300 μM ACh (0.1 s, 20 p.s.i.) typically evoked maximal currents in previous experiments and therefore provide a measure of nAChR number. ACh evoked inward currents in 100% (8/8) and 92% (11/12) of neurons transfected with α4-eGFP β4wt and α4-eGFP β4R348C nAChRs, respectively (Fig. 6, *B* and *E*). The α4-eGFP β4R348C nAChR currents (120 ± 33 pA, $n = 12$) were only 40% of α4-eGFP β4wt nAChR currents (310 ± 72 pA, $n = 8$) ($p = 0.02$) (Fig. 6*C*). Because variations among the size of neurons could complicate the data, we calculated current density (ACh currents divided by membrane capacitance). The current density of α4-eGFP β4R348C nAChRs (6.3 ± 1.4 pA/pF, $n = 12$) was 38% that of the α4-eGFP β4wt nAChRs (16.3 ± 2.1 pA/pF, $n = 8$) ($p = 0.001$) (Fig. 6*F*). Thus, in cortical neurons, the R348C mutation produces a fairly consistent ~2-fold decrease in α4β4-insertion rate and ~2.5-fold decrease in ACh-induced currents.

Chronic Exposure to Submicromolar Nicotine Increases Insertion of α4β2 nAChRs—Nicotine acts as a pharmacological chaperone for the assembly of some subtypes of nicotinic receptors such as α4β2. Previous electrophysiological, biochemical, and fluorescence-based measurements demonstrate that the exposure to nicotine concentrations like those in the brains of smokers increases the numbers of receptors on the PM (8, 35). However, less is known about the effects of nicotine on α4β4. To determine whether nicotine has a similar effect on the rate of trafficking of α4β4 receptors, we performed TIRF-based vesicle insertion measurements using α4-SEP β4 nAChRs. In Fig. 7, counting the number of insertion events as described previously shows that nicotine has no effect on the insertion rate of α4β4 nAChR-containing vesicles. This suggests that nicotine likely does not act as a chaperone helping the assembly of this nAChR subtype.

To extend previous results on nicotine-mediated α4β2 up-regulation, we also performed PM insertion studies on α4-SEP β2 nAChRs. First, we found that a greater fraction of α4-SEP β2 nAChRs reside in neutral compartments in dendritic processes (fluorescence at pH 5.4/fluorescence at pH 7.4 = 0.61), presumably because α4β2 nAChRs exit the ER rather inefficiently (8). This shows that a significantly higher portion of the α4β2 receptors are in the ER, compared with α4β4 receptors (supplemental Figs. S1 and S3). Observations of insertion events in α4β2 are complicated by this much larger population of ER resident receptors that exist both in the soma and the processes as compared with α4β4. Nonetheless, we found additional contrast to the data for α4β4 nAChRs. Experiments performed on α4β2 show that chronic nicotine (200 nM for 24 h) results in a ~2-fold increase in observed insertion events at the membrane (Fig. 7*B*). Similar to the insertion events observed for α4β4, those in cortical neurons with α4β2 are primarily transient lasting for less than a second. It has been suggested that nicotine preferentially assembles α4β2 receptors with a $(\alpha4)_2(\beta2)_3$ stoichiometry and furthermore chaperones these receptors through the secretory pathway, resulting in receptor up-regulation at the PM (8). Although these experiments show that the well established up-regulation of α4β2 does indeed involve an increased number of insertion events in the dendritic processes, they are uninformative with respect to redistribution of receptor stoichiometries.

Additional experiments examined the effect of acute nicotine at a higher concentration (1 μM) on α4β4 receptors as well. Although these receptors were not up-regulated, we did observe a reduction of the number of receptors in the mem-

brane as observed by a loss of fluorescence from the SEP fluorophore giving an F_{nic}/F_0 of 65 ± 3% (supplemental Fig. 4).

DISCUSSION

The fusion of superecliptic phluorin to the C terminus of the α4 nAChR subunit provides the means to observe receptor delivery to, and perhaps retrieval from, the PM. These labeled α4 subunits do produce nAChRs with modest functional deficit (Fig. 1), but their general behavior is consistent with that of the previously studied, fully functional subunits containing fluorescent protein inserted in the intracellular M3-M4 loop (8–10, 42, 43).

The pH sensitivity of SEP allowed us to directly visualize nAChR-containing vesicles arriving at the PM (Figs. 3 and 4) and also to examine subcellular distributions by selectively eliminating the emission from receptors residing at the PM (Fig. 2). We utilized these new constructs to examine differences in trafficking as affected by two conditions as follows: R348C, a mutant that has been associated with sporadic ALS, and by incubation in low concentrations of nicotine.

Wild Type β2 and β4 Subunits Produce Distinct Distributions in Neurons—Comparing images of α4β4 at both pH 5.4 and 7.4 shows that a majority of the fluorescence visible in TIRF is generated from PM resident receptors rather than those in the ER (Fig. 2). The dendrites and soma differ in their patterns of nAChR localization. Acidification of the extracellular solution almost completely eliminated fluorescence in dendrites, indicating that the vast majority of receptors reside on the membrane (Fig. 2). However, a large population of α4β2 is still maintained in dendritic and somatic ER.

ALS-associated β4 Subunit Mutation Affects α4β4 Trafficking—The β4R348C mutation yields reduced agonist-induced currents as compared with wild type receptor, suggesting that either trafficking to the PM is hindered or the gating of individual receptors is compromised (28). Although in all studies cortical neurons transfected with α4-SEP β4wt exhibited higher average fluorescence intensities in both the cell body and processes as compared with those transfected with α4-SEP β4R348C, these results were too variable for systematic study.

Recently, targeted mutations in the β2 subunit led to increased trafficking out of the ER and greater expression at the PM (8). In part, these studies mutated the β2 subunit to mimic the L*X*M motif found in β4, showing that this motif is a key part of the sequence interacting with cellular machinery to permit trafficking through the secretory pathway. The β4R348C mutation is adjacent to this L*X*M motif. A disruption in the amino acid sequence close to an important export motif could potentially disrupt its normal function.

Trafficking out of the ER also plays a major role in nicotine-induced up-regulation of α4β2 receptors, as assessed by changes in the number of ERES (8). We now find a reduced number of ERES for the mutant β4 as compared with the wild type subunit. Formation of ERES is in part dictated by the amount of cargo requiring transport, which suggests here that the mutant β4 interrupts trafficking early in the secretory pathway likely just after receptors are assembled in the ER. This conclusion is bolstered by additional experiments that showed no modification of the size or brightness of the *trans*-Golgi network, labeled with galactosyltransferase-mCherry, when we compared cortical neurons transfected with wild type and mutant β4 (data not shown).

To determine whether the mutation in the M3-M4 loop of β4 led to differences in trafficking dynamics, we also examined the frequency with which nAChR transport vesicles arrived at the PM. Monitoring the rate of insertion for both α4-SEP β4wt and α4-SEP β4R348C revealed differential PM insertion dynamics. Wild type receptors exhibited almost twice the insertion rate of the mutant receptors in dendritic processes (Fig. 3). Additionally, measurements of the average intensity of insertion events also revealed that vesicles carrying wild type nAChRs had modestly more receptors than those carrying the mutant. Together, these data show that the increase in ERES correlates with improved trafficking of receptors to the PM. Agonist evoked currents of the mutant receptor were ~2.5-fold smaller than for the wild type receptor (Fig. 6), compatible with our fluorescence measurements. The similarly reduced electrophysiological response and insertion rates suggest that the mutation alters trafficking and not gating of these receptors. The 2–3-fold differences observed here do not match the 10-fold loss of currents seen in previous studies in a clonal cell line (28). Evidently the effect of the mutations depends on the repertoire of associated molecules present in the host cell; perhaps the present neuronal system has more relevance.

Although the observed vesicle trafficking events mediate the insertion of nAChRs into the PM, other factors such as the duration of this interaction also influence the number of receptors inserted into the PM. One possibility is that transient interaction of the trafficking vesicle with the PM allows only a fraction of the receptors to insert per vesicle fusion. Like those seen in Fig. 3, the majority of insertion events is transient. The observed event interacted with the PM for <0.5 s before recycling away from the PM. The intensity of the insertion events for the wild type construct is 25% larger than for the mutant construct, suggesting that under favorable circumstances the vesicle can be loaded with additional nAChR cargo molecules.

Persistent events were also observed. Some insertions lasted for more than a second and in the final frames can be seen to grow dimmer as the receptors are diluted by diffusion away from the insertion point (Fig. 4). During these events, vesicles evidently deposit their entire cargo of receptors into the PM. The low frequency of these sustained events vitiated systematic study of their time course. However, the percentage of persistent events was similar for wild type, indicating that the mutation does not affect the type of vesicle insertion events into the PM. Rather, the mutation causes a generalized reduction in the number of vesicles in the secretory pathway. The presence of ERES in the processes of neurons indicates that receptors are likely assembled in the dendritic ER and subsequently inserted. The contrast between the duration of insertion events suggests that the more transient, but more frequent, interaction does not deposit the entire load of receptors contained in the vesicle.

Nicotine Incubations Increased α4β2 but Not α4β4 nAChR Insertions—α4β4* nAChRs are expressed at relatively low levels in the brain, for instance in the medial habenula-inter-

peduncular nucleus pathway (44). As such, little work has been done on the up-regulation of these receptors as compared with $\alpha4\beta2$. ALS has been linked to the degeneration of cortical neurons as well as spinal motor neurons.

To determine whether chronic nicotine has a differential affect on $\alpha4\beta2$ and $\alpha4\beta4$ receptors, we exposed cortical neurons expressing each set of subunits to 200 nM nicotine for 24 h. Under these conditions, nicotine does not affect the number of insertion events for $\alpha4\beta4$. Several previous studies show that $\alpha4\beta4$ nAChRs are not substantially up-regulated at the PM by nicotine. A constant population of receptors at the PM could potentially mask similar rates of insertion and endocytosis. Our data show, however, that the simplest explanation is probably correct; chronic incubation in nicotine does not alter the insertion of $\alpha4\beta4$ nAChRs.

In contrast, $\alpha4\beta2$ nAChRs exhibited an almost 2-fold increase in the number of insertion events in the presence of chronic nicotine. Recently, nicotine has been shown to result in an increase in ERES in Neuro-2a cells transfected with $\alpha4\beta2$. Interestingly, we have now also shown that the $\beta4$R348C mutation results in a reduction of ERES that correlates with a reduction in the trafficking of receptors to the PM. Nicotine clearly affects the trafficking of $\alpha4\beta2$, supporting the hypothesis that it acts as a pharmacological chaperone to increase the number of receptors leaving the ER, which correspondingly leads to increased ERES. The increased trafficking from the ER results in higher expression at the PM, which has been widely shown in both fluorescence and electrophysiologically based studies. Based solely on our trafficking studies, our data do not support the idea that $\alpha4\beta4$ undergoes up-regulation or that nicotine acts as a chaperone for these receptors.

In summary, our results indicate that the point mutation in the M3-M4 loop of $\beta4$ alters the trafficking of these receptors early in the secretory pathway. However, $\alpha4\beta2$, but not $\alpha4\beta4$, insertions are affected by nicotine. The results provide insight into the trafficking of nAChRs and suggest a potential mechanism for the role of nicotinic receptors in ALS.

REFERENCES

1. McGehee, D. S., and Role, L. W. (1995) *Annu. Rev. Physiol.* **57,** 521–546
2. Graham, A. J., Ray, M. A., Perry, E. K., Jaros, E., Perry, R. H., Volsen, S. G., Bose, S., Evans, N., Lindstrom, J., and Court, J. A. (2003) *J. Chem. Neuroanat.* **25,** 97–113
3. Cadugan, D. J., and Auerbach, A. (2010) *Biophys. J.* **99,** 798–807
4. Xiao, C., Nashmi, R., McKinney, S., Cai, H., McIntosh, J. M., and Lester, H. A. (2009) *J. Neurosci.* **29,** 12428–12439
5. Wu, J., George, A. A., Schroeder, K. M., Xu, L., Marxer-Miller, S., Lucero, L., and Lukas, R. J. (2004) *J. Pharmacol. Exp. Ther.* **311,** 80–91
6. Kuryatov, A., Luo, J., Cooper, J., and Lindstrom, J. (2005) *Mol. Pharmacol.* **68,** 1839–1851
7. Sallette, J., Pons, S., Devillers-Thiery, A., Soudant, M., Prado de Carvalho, L., Changeux, J. P., and Corringer, P. J. (2005) *Neuron* **46,** 595–607
8. Srinivasan, R., Pantoja, R., Moss, F. J., Mackey, E. D., Son, C. D., Miwa, J., and Lester, H. A. (2011) *J. Gen. Physiol.* **137,** 59–79
9. Son, C. D., Moss, F. J., Cohen, B. N., and Lester, H. A. (2009) *Mol. Pharmacol.* **75,** 1137–1148
10. Nashmi, R., Dickinson, M. E., McKinney, S., Jareb, M., Labarca, C., Fraser, S. E., and Lester, H. A. (2003) *J. Neurosci.* **23,** 11554–11567
11. Grailhe, R., de Carvalho, L. P., Paas, Y., Le Poupon, C., Soudant, M., Bregestovski, P., Changeux, J. P., and Corringer, P. J. (2004) *Eur. J. Neurosci.* **19,** 855–862
12. Miesenböck, G., De Angelis, D. A., and Rothman, J. E. (1998) *Nature* **394,** 192–195
13. Mani, M., and Ryan, T. A. (2009) *Front. Neural Circuits* **3,** 1–9
14. Jaskolski, F., Mayo-Martin, B., Jane, D., and Henley, J. M. (2009) *J. Biol. Chem.* **284,** 12491–12503
15. Jacob, T. C., Bogdanov, Y. D., Magnus, C., Saliba, R. S., Kittler, J. T., Haydon, P. G., and Moss, S. J. (2005) *J. Neurosci.* **25,** 10469–10478
16. Araki, Y., Lin, D. T., and Huganir, R. L. (2010) *Proc. Natl. Acad. Sci. U.S.A.* **107,** 11080–11085
17. Lin, D. T., Makino, Y., Sharma, K., Hayashi, T., Neve, R., Takamiya, K., and Huganir, R. L. (2009) *Nat. Neurosci.* **12,** 879-U887
18. Connor, J. X., Boileau, A. J., and Czajkowski, C. (1998) *J. Biol. Chem.* **273,** 28906–28911
19. Bueno, O. F., Robinson, L. C., Alvarez-Hernandez, X., and Leidenheimer, N. J. (1998) *Mol. Brain Res.* **59,** 165–177
20. Kittler, J. T., Wang, J., Connolly, C. N., Vicini, S., Smart, T. G., and Moss, S. J. (2000) *Mol. Cell. Neurosci.* **16,** 440–452
21. Xu, J., Zhu, Y., and Heinemann, S. F. (2006) *J. Neurosci.* **26,** 9780–9793
22. Fucile, S., Palma, E., Martinez-Torres, A., Miledi, R., and Eusebi, F. (2002) *Proc. Natl. Acad. Sci. U.S.A.* **99,** 3956–3961
23. David-Watine, B., Shorte, S. L., Fucile, S., de Saint Jan, D., Korn, H., and Bregestovski, P. (1999) *Neuropharmacology* **38,** 785–792
24. Simpson, C. L., and Al-Chalabi, A. (2006) *Biochim. Biophys. Acta* **1762,** 973–985
25. Sutedja, N. A., Veldink, J. H., Fischer, K., Kromhout, H., Heederik, D., Huisman, M. H., Wokke, J. H., and van den Berg, L. H. (2009) *Amyotroph. Lateral. Scler.* **10,** 302-U309
26. Ziemann, U., Winter, M., Reimers, C. D., Reimers, K., Tergau, F., and Paulus, W. (1997) *Neurology* **49,** 1292–1298
27. Thorns, J., Wieringa, B. M., Mohammadi, B., Hammer, A., Dengler, R., and Münte, T. F. (2010) *Exp. Neurol.* **224,** 389–394
28. Moriconi, C., Di Angelantonio, S., Piccioni, A., Trettel, F., Sabatelli, M., and Grassi, F. (2011) *Pflügers Arch. Eur. J. Physiol.* **461,** 225–233
29. Sabatelli, M., Eusebi, F., Al-Chalabi, A., Conte, A., Madia, F., Luigetti, M., Mancuso, I., Limatola, C., Trettel, F., Sobrero, F., Di Angelantonio, S., Grassi, F., Di Castro, A., Moriconi, C., Fucile, S., Lattante, S., Marangi, G., Murdolo, M., Orteschi, D., Del Grande, A., Tonali, P., Neri, G., and Zollino, M. (2009) *Hum. Mol. Genet.* **18,** 3997–4006
30. Lin, L., Jeanclos, E. M., Treuil, M., Braunewell, K. H., Gundelfinger, E. D., and Anand, R. (2002) *J. Biol. Chem.* **277,** 41872–41878
31. Ren, X. Q., Cheng, S. B., Treuil, M. W., Mukherjee, J., Rao, J., Braunewell, K. H., Lindstrom, J. M., and Anand, R. (2005) *J. Neurosci.* **25,** 6676–6686
32. Kauer, J. A., and Malenka, R. C. (2007) *Nat. Rev. Neurosci.* **8,** 844–858
33. Kalivas, P. W. (2009) *Nat. Rev. Neurosci.* **10,** 561–572
34. Ritz, B., Ascherio, A., Checkoway, H., Marder, K. S., Nelson, L. M., Rocca, W. A., Ross, G. W., Strickland, D., Van Den Eeden, S. K., and Gorell, J. (2007) *Arch. Neurol.* **64,** 990–997
35. Buisson, B., and Bertrand, D. (2001) *J. Neurosci.* **21,** 1819–1829
36. Nelson, M. E., Kuryatov, A., Choi, C. H., Zhou, Y., and Lindstrom, J. (2003) *Mol. Pharmacol.* **63,** 332–341
37. Lester, H. A., Xiao, C., Srinivasan, R., Son, C. D., Miwa, J., Pantoja, R., Banghart, M. R., Dougherty, D. A., Goate, A. M., and Wang, J. C. (2009) *AAPS J.* **11,** 167–177
38. Stephens, D. J., Lin-Marq, N., Pagano, A., Pepperkok, R., and Paccaud, J. P. (2000) *J. Cell Sci.* **113,** 2177–2185
39. Asokan, A., and Cho, M. J. (2002) *J. Pharm. Sci.* **91,** 903–913
40. Cheng, S. B., Amici, S. A., Ren, X. Q., McKay, S. B., Treuil, M. W., Lindstrom, J. M., Rao, J., and Anand, R. (2009) *J. Biol. Chem.* **284,** 23251–23259
41. Khakh, B. S., Fisher, J. A., Nashmi, R., Bowser, D. N., and Lester, H. A. (2005) *J. Neurosci.* **25,** 6911–6920
42. Nashmi, R., Xiao, C., Deshpande, P., McKinney, S., Grady, S. R., Whiteaker, P., Huang, Q., McClure-Begley, T., Lindstrom, J. M., Labarca, C., Collins, A. C., Marks, M. J., and Lester, H. A. (2007) *J. Neurosci.* **27,** 8202–8218
43. Drenan, R. M., Nashmi, R., Imoukhuede, P., Just, H., McKinney, S., and Lester, H. A. (2008) *Mol. Pharmacol.* **73,** 27–41
44. Grady, S. R., Moretti, M., Zoli, M., Marks, M. J., Zanardi, A., Pucci, L., Clementi, F., and Gotti, C. (2009) *J. Neurosci.* **29,** 2272–2282

Neurobiology:

Trafficking of α4* Nicotinic Receptors Revealed by Superecliptic Phluorin: EFFECTS OF A β4 AMYOTROPHIC LATERAL SCLEROSIS-ASSOCIATED MUTATION AND CHRONIC EXPOSURE TO NICOTINE

Christopher I. Richards, Rahul Srinivasan, Cheng Xiao, Elisha D. W. Mackey, Julie M. Miwa and Henry A. Lester

J. Biol. Chem. 2011, 286:31241-31249.
doi: 10.1074/jbc.M111.256024 originally published online July 18, 2011